16th World Conference on Earthquake, 16WCEE 2017
Santiago Chile, January 9th to 13th 2017
Paper N° 4603
Registration Code: S-Z1464752185

FAILURE MODES OF STARRED ANGLE BRACES

F. Claverie[(1)], R. Herrera[(2)]

[(1)] Graduate Research Assistant, Dept. of Civil Engineering, University of Chile, Santiago, Chile, fabbio.claverie@ug.uchile.cl
[(2)] Assistant Professor, Dept. of Civil Engineering, University of Chile, Santiago, Chile, riherrer@ing.uchile.cl

Abstract

One of the most used structural steel systems in industrial structures in Chile is the Concentrically Braced Frame (CBF). Among the shapes used as braces, a common choice before 2010 was the use of starred angles (or XL shapes). This is a built-up shape composed of two angles joined intermittently at the heels, forming a cross-shaped section. Starred angles have several advantages: they are simple to fabricate, easy to install on the frame, and their configuration makes clean up and maintenance less complicated. However, a number of these braces failed during the 2010 Maule earthquake in Chile. Failures observed included local buckling, lateral torsional buckling, and connection fractures. These failures, although not yet completely explained, have made engineers steer away from the use of starred angles as braces.

This work presents a numerical study on the failure modes of starred angle braces in X configuration, made up from commercially available angle shapes. Finite element models of different brace configurations are built considering initial imperfections, nonlinear material behavior and large deformations. Gusset plates and stitch plates are also modeled and contact conditions established between these elements and the angles. The models are subjected to cycles of increasing displacement amplitude. Results for axial load capacity, hysteresis loops, failure mode, and forces between the gusset plates and stitch plates and the angles are extracted from the analysis.

The results indicate that the global buckling failure mode (flexural, torsional, or flexural-torsional) developed by the brace depends on its size. In addition, for some cases the forces developed in the connections between the stitch plates and gusset plates and the angles, are larger than the forces normally used to design these connections, which could explain the failures observed after the earthquake.

Keywords: Starred angle braces; Built-up brace; Concentrically braced frame; Flexural torsional buckling.

1. Introduction

The vast majority of steel structures in Chile are industrial facilities, which are commonly structured with concentrically braced frames (CBF) and moment resisting frames (MRF). The seismic design of industrial facilities is ruled by the code NCh2369 [1], which contains design considerations based in great extent on the AISC LRFD Specification [2]and the AISC Seismic Provisions [3], complemented with empirical recommendations of the leading structural design offices of industrial facilities in the country, gathered mainly in the second half of the 20th century. This methodology has provided satisfactory structural performance for both the 1985 Valparaiso earthquake and the 2010 Maule earthquake. Nonetheless, in thone latter, several failures were observed, corresponding the most critical cases to facilities older than 20 years designed without stringent ductility and overstrength requirements, which included cellulose pulp mills, steel mills, wine production facilities, and cement plants [4][5].

Among the most observed failures were brace instabilities. Braces restrict frame lateral displacements, resisting during seismic events alternating tensile and compressive forces. One of the most affected shapes used as braces were the starred angles, exhibiting failures as local buckling, flexural torsional buckling and connection fractures (Fig. 1).

Fig. 1 – Failures observed on starred angle braces: a) Local buckling; b) Torsional buckling; c) Fracture on the cross point connection. ([4][5]).

Starred angles are composed of two angles joined intermittently at the heels, forming a cross-shaped section. Further keeping the angles together, the interconnection plates (stitch plates) have as function to prevent the angles distortion due to the applied load. Moreover, the number and type of interconnectors have a significant effect on the behavior of this built-up section, mainly on its compressive strength, buckling axis, and fracture life [4].

Several experimental and analytical studies have been carried out to understand the inelastic response of bracing steel members although most of them focus on RHS, CHS and W-shapes. Despite this, it is well-known that key parameters that influence the braces behavior are their effective slenderness and the compactness of their cross section. Molina [5], by means of a numerical study determined that the failure modes of starred angles under monotonically increasing compression could be adequately sorted according to their slenderness-compactness ratio: elements with ratios lesser than 5.5 experienced torsional buckling, while elements with greater ratios were likely to develop flexural buckling.

A similar procedure is conducted herein, to assess the relation between the size of the brace and its failure mode, under cyclic loading. Other parameters examined are: the axial load capacity, hysteresis loops, and forces in the gusset connection and in the central connection (diagonal intersection). 74 configurations of different lengths and sections were modeled using the finite element software ANSYS Workbench 15. The selection of the sections was made according to NCh2369 [1] requirements, using commercially available rolled equal-leg

angle shapes. The angles ranged from 40 to 200 mm flange width and from 4 to 16 mm thickness, while the length of the braces varied from 3000 to 6000 mm.

Additionally, two different separations of stitch plates were used: one of them following the dimensional requirements for built-up sections from the AISC360-10 [8] which led, roughly, to interconnectors situated at the quarter points of the total brace length. On the other hand, the dimensional requirements for special concentrically braced frame diagonals (SCBF) from AISC341-10 [9] lead, approximately, to stitch plates located at half that distance. Therefore, $L_B/4$ and $L_B/8$ were the arrangements of interconnectors studied herein, where L_B is the total brace length.

2. Finite Element Model

The finite element analysis was performed in two stages. The first stage was an elastic buckling analysis, conducted to obtain the elastic buckling mode and critical load. Then, an initial imperfection proportional to the elastic buckling mode was created in the specimen to generate a small camber and guide the buckling mode in the non-linear analysis (second stage).

2.1. Geometry

Gusset plates were modeled considering simplifications on their geometry: the free length was taken as two times their thickness in order to provide space long enough to permit plastic rotations, yet short enough to avoid the occurrence of gusset buckling prior to brace buckling [10], this because braces which undergo cyclic deformations under severe ground motions may develop plastic hinges at their center and at each end. The plate height was determined so that the Whitmore section [11] could fully develop, while a capacity design was used to determine its thickness: the connections were designed to resist a tension force equal to $R_yF_yA_g$ and a compression force equal to the lesser of $R_yF_yA_g$ and $1.14F_{cr}A_g$ (with F_{cr} calculated using R_yF_y in lieu of F_y), as stated in the AISC seismic provisions. In these expressions R_y is the ratio of the expected yield stress to the specified minimum yield stress (R_y=1.5 for hot-rolled structural shapes made of ASTM A36 steel). Regarding the stitch plates, they were modeled with the same height of the starred angle section and 2/3 of the section height in length [12] (Fig. 2).

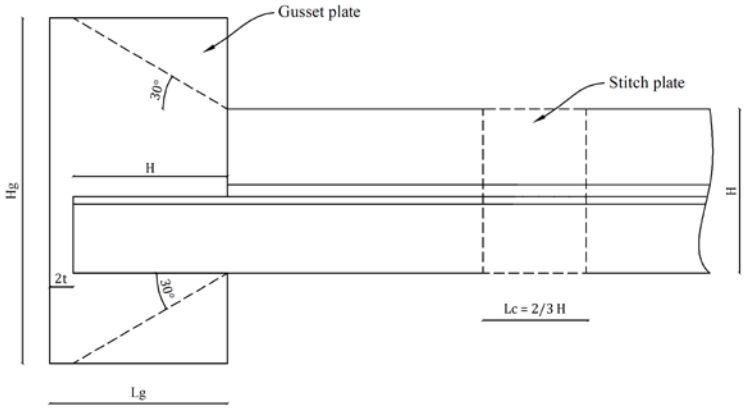

Fig. 2 – Geometry of a modeled brace with gusset and stitch plates included.

2.2. Material and contacts

Both the angles and plates (gusset and interconnectors) were made of ASTM A36 steel (see material properties in Table 1). Additionally, a bilinear constitutive law with isotropic strain hardening was established to characterize the nonlinear behavior of the material.

Each specimen consists of three components: angles, gusset plates and stitch plates, interacting through contact conditions. The contact established between the different components was of the *bonded* type [13], i.e., without relative displacements or separation between the interacting components. This condition simulates adequately a welded connection, where the parts remain fixed. The pieces in contact are modeled as *contact* and

target pairs, where *contact* elements penetrate *target* elements due to their higher relative stiffness. Given that all pieces are made of the same material, the specification for which each component take the *contact* or *target* role was selected as controlled by the program.

Table 1 – Material properties

Steel type	ASTM A36
ρ [kgf/m^3]	7850
E [GPa]	200
F_y [MPa]	250
F_u [MPa]	460
Tangent modulus [MPa]	10000

2.3. Meshing and initial imperfection

For the meshing, a twenty-node three dimensional brick element was used. A sensibility analysis was conducted in order to determine the maximum size of the edges, studying as parameter the axial deformation at first significant yield, δ_y. The analysis prioritized obtaining the most accurate results with the least overall convergence time, but given the lack of experimental data to contrast with the sensibility analysis, results from a hyper-fine meshing configuration were employed.

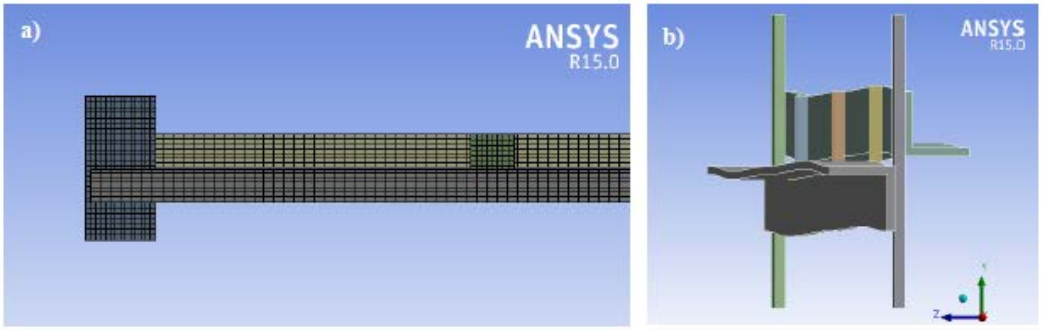

Fig. 3 – Finite element model: a) Mesh applied on an element; b) Initial imperfection due to a flexural buckling mode.

Regarding the initial imperfection, it ranged from L_B/600 to L_B/1200, with a maximum camber of 5 mm, determined by means of a sensibility analysis with δ_y as studied parameter, just as conducted to establish the mesh refinement. Figs. 3a and 3b show the mesh applied on a model and its initial camber, respectively.

2.4. Boundary conditions

Braces were modeled in isolation, therefore boundary conditions shall simulate appropriately an X configuration. This was achieved by imposing constraints on the central interconnection plate to represent the braces intersection. The seismic code for industrial facilities used in Chile [1] states that when X configurations are employed, the braces must be interconnected at the intersection and the point of intersection considered as braced out-of-plane. Fig. 4 shows the point where restrictions were applied as well as the global axes, whereas Table 2 shows the constraints. Both the central stitch plate and one of the ends (where loading history acts) have only longitudinal displacement released, the other end is considered fixed instead. Thus, the gusset plate rotation is subjected to its own rotational stiffness, considering that enough space to allow inelastic rotation and hinging due to the brace out-of-plane buckling was provided.

Table 2 – Brace boundary conditions (R=Restrained, F=Free).

			Restraint			
Remote Displacement	Disp. X	Disp. Y	Disp. Z	Rot. X	Rot. Y	Rot. Z
A (Left end)	R	R	R	R	R	R

B (Intersection)	F	R	R	R	R	R
C (Right end)	F	R	R	R	R	R

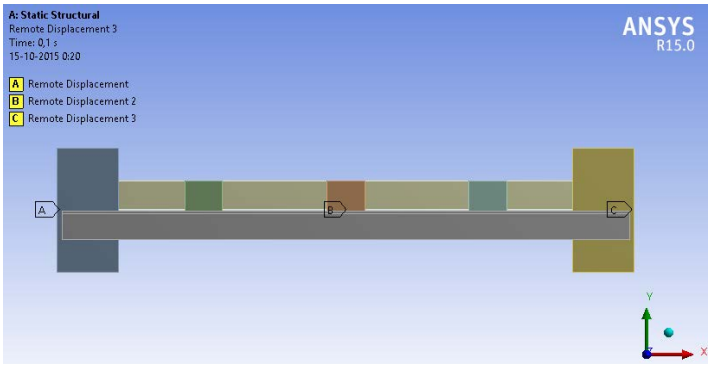

Fig. 4 – Points where boundary conditions were applied.

2.5. Loading history

A quasi-static cyclic analysis was conducted, the displacement pattern was symmetrical with the amplitude of the excursions in tension and compression increasing stepwise every second cycle (see Fig. 5). The maximum amplitude was taken as $4\delta_y$ based on NEHRP Recommended Seismic Provisions [12], where the yield displacement, δ_y, was determined from the Von Mises equivalent stress- equivalent deformation curves and taken as the displacement which caused (in compression) the first significant alteration in the elastic slope. The δ_y values ranged from 1.5 mm to 4 mm and were roughly equal to $KL\varepsilon_y$, with a mean calculated-to-predicted ratio of 0.99 and a standard deviation of 0.13. The loading history has a total accumulated deformation of $84\delta_y$, where $72\delta_y$ correspond to inelastic excursion.

Even though the ductility level imposed by the cyclic load is μ: δ/δ_y = 4, some elements exceeded the tensile strength (F_u = 460 MPa) at lower deformation levels ($3\delta_y<\delta\leq4\delta_y$). A limit stress associated with fracture was therefore applied, amplifying the nominal tensile strength by a factor of 1.09, i.e., allowing a tensile strength of 500 MPa to be attained. Thereby, a larger correlation with an eventual fracture in practice can be assured, since ultimate strengths are firstly reached in the model on highly localized zones, so using a unitary factor would lead to an early analysis termination. A monotonic analysis was also performed on each model for comparison purposes. Results for axial load capacity, hysteresis loops, failure mode, and forces between the gusset plates, stitch plates and angles were extracted from both analyses.

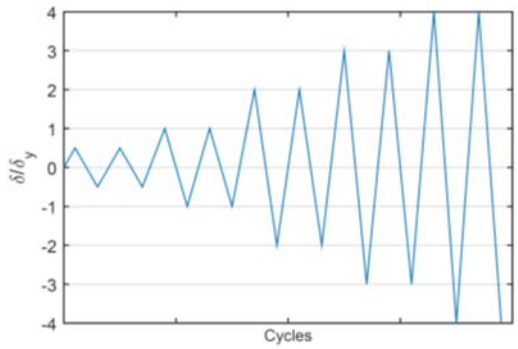

Fig. 5 – Loading history.

3. Results

3.1 Axial load capacity

Fig. 6a shows the maximum compressive strength (C_u) divided by the yield capacity for both the monotonic and the cyclic analyses. It can be seen that C_u values from the cyclic analysis exceed slightly the C_u values obtained from the monotonic ones (11% in average). Likewise, the maximum compressive strengths due to monotonic loading are larger (22% in average, accentuated in stockier braces prone to develop torsional buckling) than the nominal values obtained from Chapter E of AISC360-10 [8].

On the other hand, the maximum tensile strength achieved by the braces ranged from $1.1F_yA_g$ in more slender elements, up to $1.3F_yA_g$ in the stockier ones, decreasing with increasing effective slenderness (see Fig. 6b).

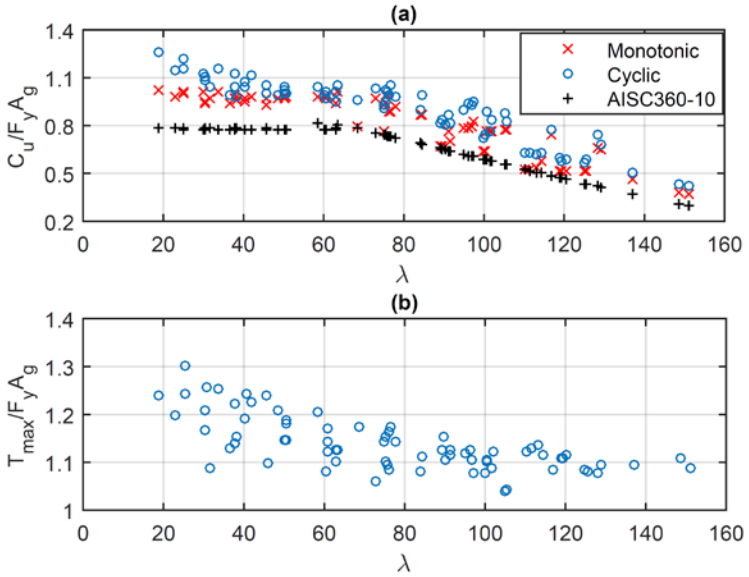

Fig. 6 – Maximum capacities: a) Compressive maximum strengths; b) Tensile maximum strengths.

3.2 Hysteresis loops

In this work, differences among the hysteresis loops were observed depending on the global buckling mode. Fig. 7 depicts the hysteretic response of a representative sample of elements depending on their failure mode: the x-axis is the ductility ratio, while the y-axis contains the axial load normalized by the yield capacity.

It can be seen From Fig. 7 that when flexural buckling occurs, the compressive resistance degrades significantly. This decrement is caused by the formation of plastic hinges near the mid-length of the unbraced points, due to the Bauschinger effect, and residual out-of-plane deformations accumulated from previous cycles [15]. In tension, the braces reached their tensile yield resistance and developed some strain hardening, achieving a maximum tensile strength T_{max} that remains practically constant in the subsequent cycles. A similar behavior is observed in the elements with flexural torsional buckling, with the exception that the monotonic curve after buckling is less tight to the cyclic curve.

On the contrary, the compressive strength degradation is considerably lower (or inexistent) in elements with torsional buckling, showing a similar response for both tensile and compressive loadings. This can be explained by considering that torsion of these elements develops without significant out-of-straightness deformation, leading to a less extent of lateral deformation and the non-formation of the plastic hinge and strain concentration in a specific zone (which produce the capacity loss). While this represents an advantage in structural terms, it implies a high cost of material since the elements with this behavior are the less slender ones.

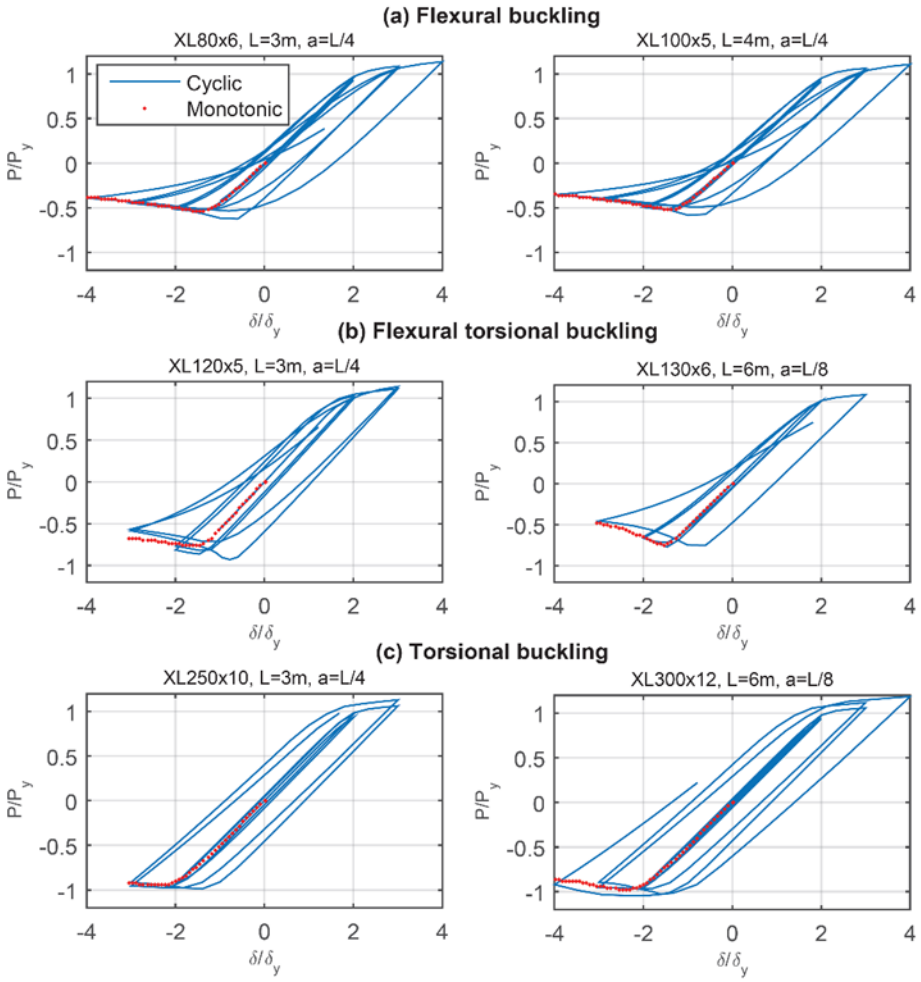

Fig. 7 – Hysteresis loops for different buckling modes.

3.3 Failure modes

From the results can be inferred that the failure modes can be linked to geometric properties. Then, in order to determine a parameter that directly encompasses both the brace length and its cross section, the following ratio is defined:

$$\lambda_{S/C} = \frac{\max(\lambda_{u,eff}; \lambda_v)}{(b/t)} \quad (1)$$

In the Eq. (1), $\lambda_{u,eff}$ is the effective slenderness with respect to the u-u axis (modified because of the stitch plates spacing) and λ_v is the v-v axis slenderness ratio, whereas *b/t* is the width-to-thickness ratio.

A clear distinction of the failure modes is observed when plotted against the slenderness-to-compactness ratio (see Fig. 8), without apparent effect from the stitch plate spacing. Elements with $\lambda_{S/C}$ ratios less than 6 were likely to develop torsional buckling, for $\lambda_{S/C}$ ratio from 6 to 10, flexural-torsional buckling tended to occur; finally if the slenderness-to-compactness ratio is greater than 10, flexural buckling develops.

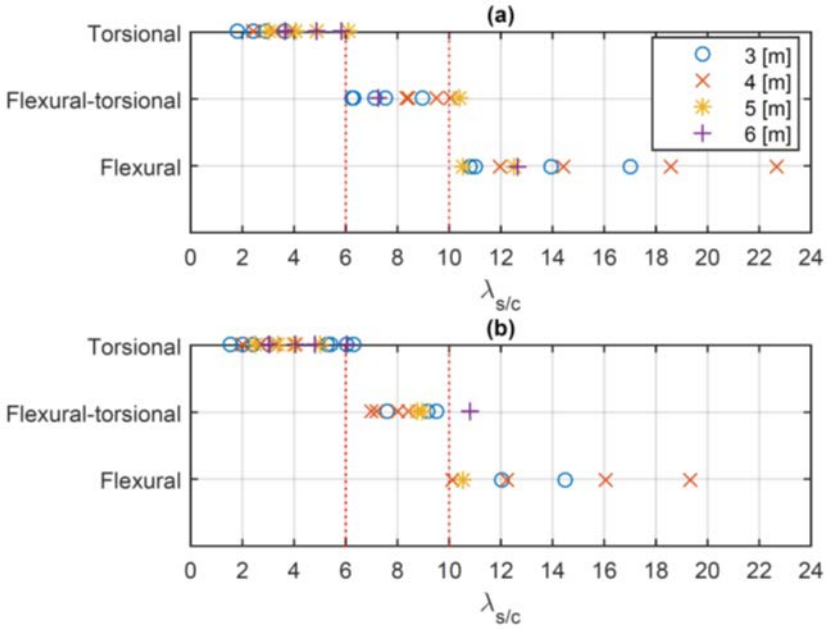

Fig. 8 – Failure modes in function of the slenderness-compactness ratio for: a) Stitch plates spaced at $L_B/4$; b) Stitch plates spaced at $L_B/8$.

3.4 Forces in the gusset plate connections

In this section, the maximum forces developed in the gusset plate connections are provided considering the decomposition shown in the Fig. 9. For the forces developed in the plane of the plate (contained in X and Y axis) both senses (negative and positive) were considered and the worst case selected, whereas just forces which implied a separation between the plate and the angle were accounted for the Z-axis forces. The forces given correspond to the maximum among the four faces of both brace ends.

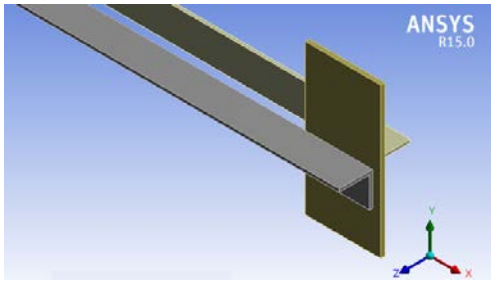

Fig. 9 – Axes of the gusset connection.

For X-axis forces and stitch plates at the quarters, no significant dependence on the failure mode is observed (Fig. 10), averaging a 40% of F_yA_g in the monotonic analysis and a 50% of F_yA_g in the cyclic analysis. When the number of interconnectors was increased, the forces raised an 11% and showed a growing trend for elements with flexural and flexural-torsional buckling ($\lambda_{S/C}$ > 6). Y-axis forces were considerably lower, reaching a 5% of the yield strength in the worst case. Finally, it can be seen that separation forces are the most demanding (exceeding F_yA_g in some cases) in elements with larger out-of-plane deformation, i.e., with flexural buckling mode. On the other hand, the Z-axis forces developed in the stockier elements within the torsional buckling branch (characterized by a slenderness-to-compactness ratio under 4) were not greater than $0.3F_yA_g$, which leads to presume that higher lateral deformations induce outward reaction forces in the gusset plate.

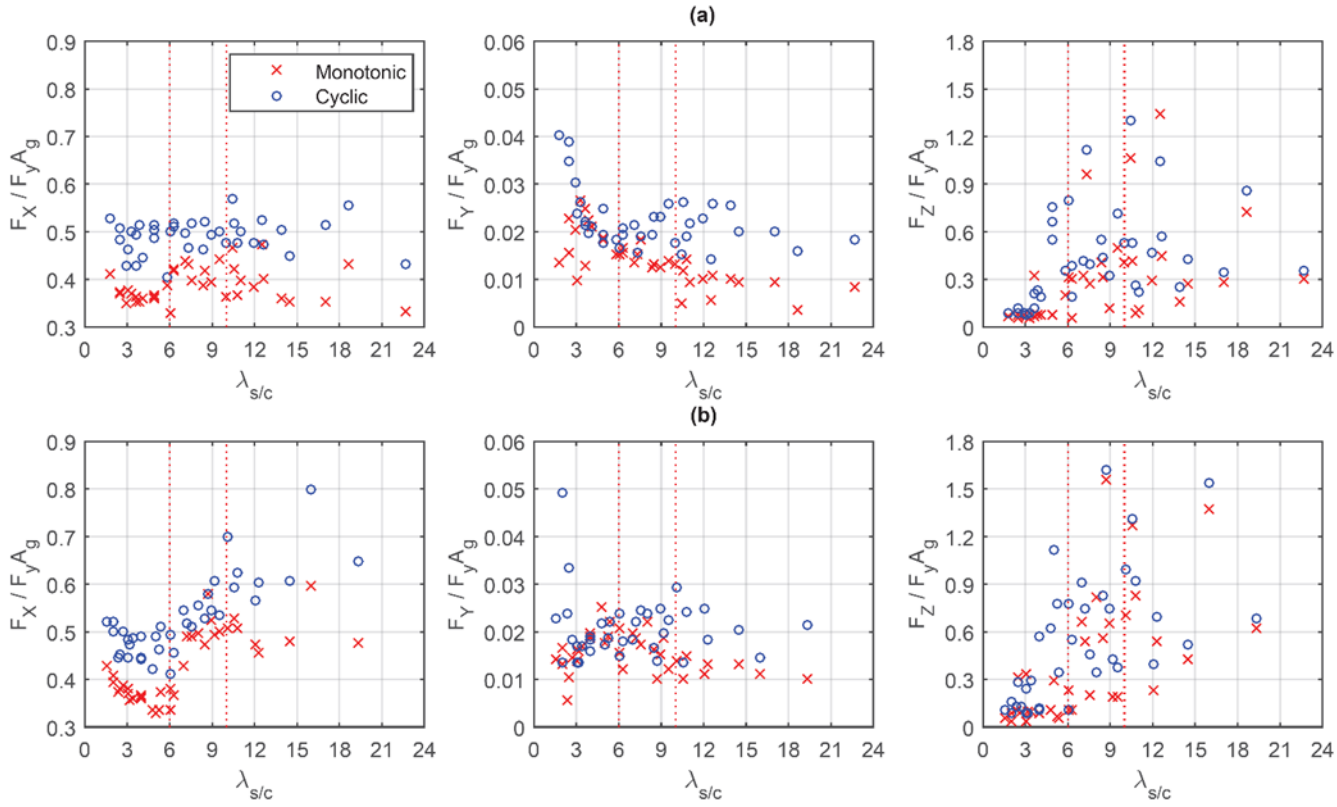

Fig. 10 – Forces developed in the gusset to angle connection, for: a) Stitch plates spaced at $L_B/4$; b) Stitch plates spaced at $L_B/8$.

3.5 Forces in the intersection connection.

The diagonals intersection may represent a highly vulnerable point within the frame, mainly because of the low importance usually given to the forces that may develop on this zone (see Fig. 1c). In order to determine the significance of such efforts, the maximum forces in the cross point (central stitch plate) were extracted from the analysis. The decomposition of the forces follows the axes shown in Fig. 11, and, similarly to the gusset connection forces, for the efforts developed in the plane of the stitch plate (contained in X and Y axis) both senses (negative and positive) were considered and the worst case selected, whereas just forces which implied a separation between the stitch plate and the angle were accounted for the Z-axis forces. The forces given correspond to the maximum between the two interconnector faces.

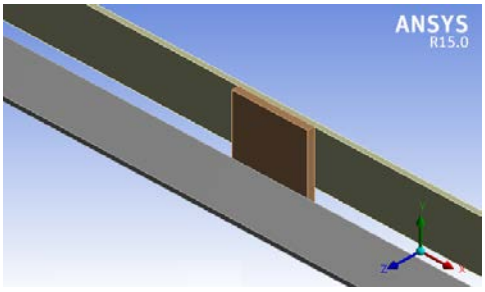

Fig. 11 – Axes of the intersection connection.

From Fig. 12 is observed that the lower X-axis forces (normalized by $F_y A_g$) belong to the torsional buckling branch (similar behavior described by the Z-axis gusset place forces), remaining under 10% of the yield strength, whereas the larger forces develop in flexural modes, reaching nearly 50% of $F_y A_g$. It is noteworthy to mention that values increased broadly at reducing the stitch plate spacing (130% in average), specially in more slender braces. The Y-axis forces reached 4% of $F_y A_g$ when $L_B/4$ spacing is used and 6% in $L_B/8$ spacing

configuration. Finally, the Z-axis forces extracted from the cyclic analysis were larger in torsional modes, decreasing for flexural-torsional and flexural modes. Forces from monotonic analysis, instead, were practically null, impliying that when pure compression is applied the central connection develops inward forces, i.e., it is crushed. In this case the arrangement of interconnectors seems not to have any influence.

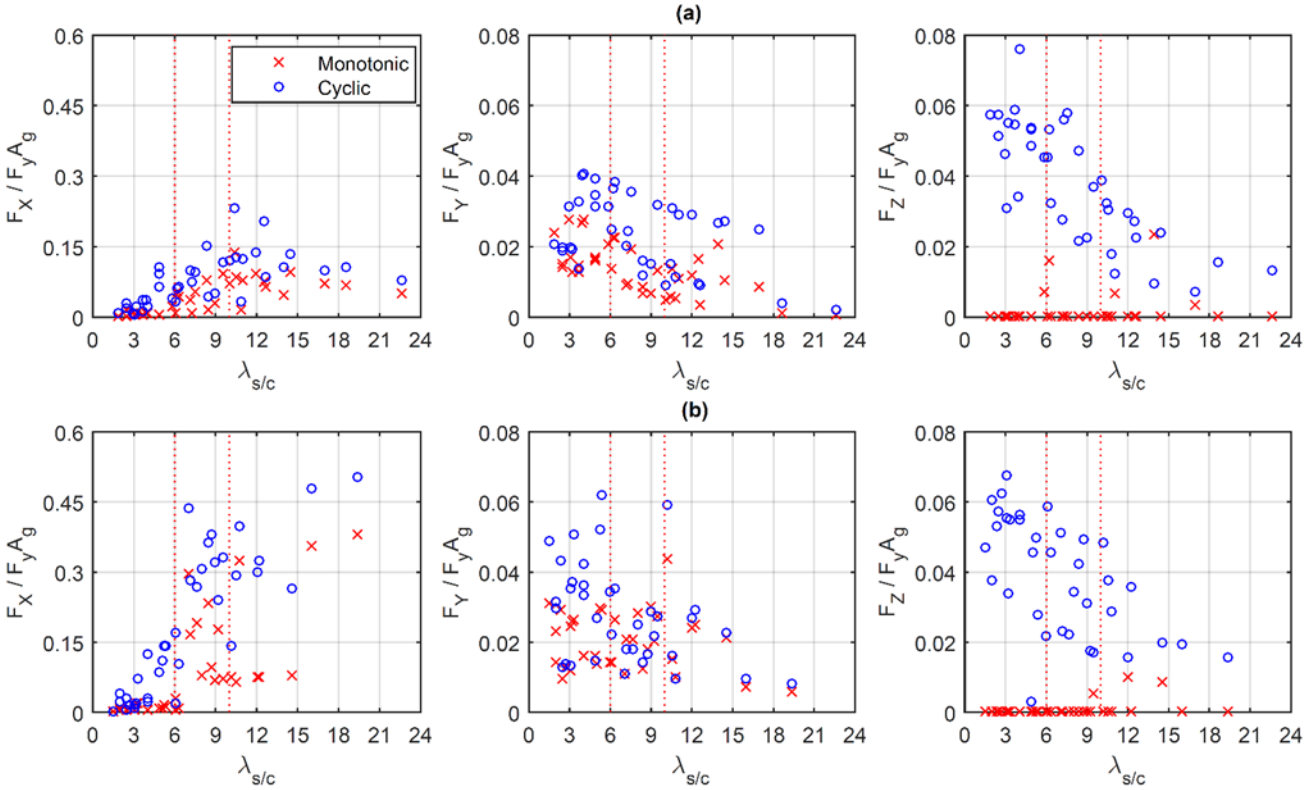

Fig. 12 - Forces developed in the cross point connection, for: a) Stitch plates at $L_B/4$; b) Stitch plates at $L_B/8$.

4. Conclusions

A numerical study on the failure modes of starred angle braces in X configuration was conducted. The sections were made up from commercially available angle shapes in Chile. Finite element models of 74 different brace configuration were built and the axial load capacity, hysteresis loops, and forces in the gusset and intersection connection were extracted from the analysis.

The maximum axial forces carried by the braces generally exceeded the expected values for both tensile and compressive loads. The maximum tensile strengths measured were in all cases larger than the yielding capacities, roughly in a 110% in elements with flexural and flexural-torsional buckling modes and a 130% in torsional failures. Additionally, the spacing of the interconnectors did not influence the tensile capacity. Regarding the compressive maximum strengths (C_u), they exceeded in a 22% (on average) the predicted value from AISC360-10 [8]. Differences between the C_u values coming from the monotonic and the cyclic analysis were also observed: the same brace subjected to cyclic loading developed, on average, an 11% higher maximum compressive strength. It is important to bear in mind that axial forces that are likely to be developed by the brace in severe ground motions may exceed the nominal strengths. The results from Fig. 6 suggest that capacities higher than the nominal must be assigned to the brace when conducting a capacity design for connection detailing purposes.

The hysteresis loops showed differences depending on the global buckling mode. In all cases, however, the maximum compressive capacity C_u was reached at first buckling occurrence. Additionally, given the shape of the cyclic loading history, the brace buckled after yielding in tension. The post-buckling compressive capacity degraded when further negative deformation was applied, mainly in elements with flexural and flexural-torsional

buckling. On the contrary, elements with torsional buckling (the less slender ones) lost their compressive capacity to a lesser extent, mainly due their negligible out-of-plane deformations.

The ratio between the effective slenderness and the width-to-thickness ratio ($\lambda_{S/C}$) is an adequate failure mode predictor: elements with $\lambda_{S/C}$ ratios lesser than 6 were likely to develop torsional buckling; when the $\lambda_{S/C}$ ratio ranged from 6 to 10, flexural-torsional buckling tended to occur; and if the slenderness-to-compactness ratio is greater than 10, flexural buckling develops.

The forces developed in both the gusset and intersection connection showed dependence on the failure mode and the spacing of the stitch plates. The most demanding forces in the gusset connection are those contained in the X and Z-axis (see Fig. 9), exceeding F_yA_g in some cases, which could explain the connection fractures observed after the 2010 Chilean earthquake. Additionally, the forces developed in the central connection shall not be neglected since values up to 50% F_yA_g were reached. In general, the usage of a high number of interconnectors led to considerably higher forces developed in the connections (mainly in the central one), therefore a quarter-point arrangement of stitch plates is recommended. Elements with flexural and flexural-torsional buckling modes experienced the most critical forces (in the most demanding axes) in their connections, however, elements with $\lambda_{S/C}$ > 10 (flexural failure), have economic advantages (lighter sections given the same brace length) and lower associated reparation costs if buckling occurs. Thus, using $\lambda_{S/C}$ values lesser than 6 and greater than 10 is recommended.

5. References

[1] INN, 2003. NCh 2369.Of2003. Earthquake resistant design of industrial structures and facilities, Instituto Nacional de Normalización, Santiago, Chile.

[2] AISC 1999. Load and resistance factor design specification for structural steel buildings, American Institute of Steel Construction, Chicago, Illinois, USA.

[3] AISC 2002. Seismic Provisions for Structural Steel Buildings, ANSI/AISC 341-02, American Institute of Steel Construction, Chicago, Illinois, USA.

[4] Montecinos, R., Herrera, R., Verdugo, A., Beltrán, J.F., 2012. Estructuras industriales, Mw=8.8 Terremoto en Chile, 27 de febrero 2010, Chapter 10, 211-239. Department of Civil Engineering, University of Chile.

[5] Herrera, R., Beltrán, J.F., 2012. Performance of steel structures during the February 27, 2010, Chile earthquake. 15th WCEE. Paper N°4249.

[6] Schepers, J.A., 1983. The interconnection of starred angle compression members. A thesis presented to the University of Windsor in partial fulfillment of the requirements for the degree of Masters of Applied Science in Civil Engineering, University of Windsor, Ontario, Canada.

[7] Molina, J., 2014. Modos de falla predominantes en perfiles XL de acero estructural, Civil Engineering Thesis, University of Chile, Santiago, Chile.

[8] AISC 2010. Specification for Structural Steel Buildings, ANSI/AISC 360-10, American Institute of Steel Construction, Chicago, Illinois, USA.

[9] AISC 2010. Seismic Provisions for Structural Steel Buildings, ANSI/AISC 341-05, American Institute of Steel Construction, Chicago, Illinois, USA.

[10] Astaneh-Asl, A., Goel, S.C., and Handon, R.D., 1986. Earthquake-resistant design of double angle bracing, Engineering Journal, AISC, Vol. 23, No.4, 4th Quarter, Chicago, IL.

[11] Whitmore, R.E., 1952. Experimental investigation of stresses in gusset plates. Masters Thesis, University of Tennessee Engineering Experiment Station Bulletin No. 16, Knoxville, USA.

[12] Vergara del Pozo, R., 2004. Manual de diseño para ángulos estructurales L-AZA. Gerdau Aza, Santiago, Chile.

[13] ANSYS Inc., 2009. Contact Technology Guide, Canonsburg, PA.

[14] Building Seismic Safety Council, 2009. NEHRP Recommended seismic provisions for new building and other structures, FEMA P-750. Washington, DC: Federal Emergency Management Agency.

[15] Tremblay, R., 2002. Inelastic seismic response of steel bracing members. Journal of Constructional Steel Research, **58:5-8**, 665-701.